18 Two-Beam Coupling and Phase Conjugation in Photorefractive Media

18.0 INTRODUCTION

In Chapter 17 we investigated the exchange of power among four optical waves at frequencies ω_1, ω_2, ω_3 that is mediated via the nonlinear optical response of the medium [see (17.2-2)]

$$P_i^{\mathrm{NL}}(\mathbf{r}) = 3\chi_{ijk\ell}^{(3)} A_{1j}(\mathbf{r}) A_{2k}(\mathbf{r}) A_{3\ell}^{*}(\mathbf{r}) e^{i[(\omega_1+\omega_2-\omega_3)t-(\mathbf{k}_1+\mathbf{k}_2-\mathbf{k}_3)\cdot\mathbf{r}]} + \text{c.c.} \qquad (18.0\text{-}1)$$

where $A_{sm}(s = 1, 2, 3)$ is the complex amplitude of the mth Cartesian component of the sth wave. The coefficient $\chi_{ijk\ell}^{(3)}$ characterizes the nonlinear polarization response of the material medium (atoms, molecules). Relation (18.0-1) is local (it involves field quantities at the point $\mathbf{r}$ only), and the coefficient $\chi_{ijk\ell}^{(3)}$ can, in principle, be obtained by solving for the (local) nonlinear response of the atoms or molecules [2]. There exists a very important class of nonlinear interactions in which the response is nonlocal. Among these the photorefractive effect and stimulated Brillouin scattering are the most important since they both lead to large effects. Both of these cases can be described by a scenario in which two of the incident waves, say 1 and 3, "write" an index of refraction grating in the medium that is proportional to their (spatially and temporally varying) intensity interference pattern.

$$\Delta n \propto A_1 A_3^{*} e^{i[(\omega_1-\omega_3)t-(\mathbf{k}_2-\mathbf{k}_3)\cdot\mathbf{r}]} + \text{c.c.}$$

The third wave at ω_2 is Bragg-scattered from the grating, resulting in the fourth wave

$$A_4 \propto \Delta n A_3 \propto A_1 A_2 A_3^{*} \exp\{i[(\omega_1+\omega_2-\omega_3)t-(\mathbf{k}_1+\mathbf{k}_2-\mathbf{k}_3)\cdot\mathbf{r}]\}$$

which has the same form as (18.0-1).

Before considering this dynamic case, we take up the simpler situation of a fixed index grating.

18.1 TWO-WAVE COUPLING IN A FIXED GRATING

We consider a two-wave optical field at a radian frequency ω

$$\mathbf{E}(\mathbf{r}) = \frac{1}{2}\mathbf{A}_1(r_1)e^{-i\mathbf{k}_1\cdot\mathbf{r}} + \frac{1}{2}\mathbf{A}_2(r_2)e^{-i\mathbf{k}_2\cdot\mathbf{r}} + \text{c.c.} \tag{18.1-1}$$

so that the complex amplitudes of the beams are $A_{1,2}$. The beam polarization is taken, for simplicity, to be perpendicular to the plane of the paper.

The two waves are propagating in a medium with a spatially periodic stationary index distribution ("grating")

$$n(\mathbf{r}) = n_0 + n_1 \cos(\mathbf{K}\cdot\mathbf{r} + \phi) \tag{18.1-2}$$

as shown in Figure 18-1.

The paraxial wave equation that is obeyed by the field (see 17.1-2) is

$$\nabla^2\mathbf{E} + \omega^2\mu\epsilon(\mathbf{r})\mathbf{E} = 0 \tag{18.1-3}$$

where the dielectric constant now has a contribution from the grating

$$\epsilon(r) = \epsilon_0 n^2(r) \cong \epsilon_0\,[n_0^2 + (n_0 n_1 e^{-i(\mathbf{K}\cdot\mathbf{r}+\phi)} + \text{c.c.})] \tag{18.1-4}$$

Substituting (18.1-1) and (18.1-2) in (18.1-3) leads to

$$\begin{aligned}
&\frac{1}{2}\left(-2ik_1\frac{dA_1}{dr_1} - k_1^2A_1\right)e^{-i\mathbf{k}_1\cdot\mathbf{r}_1} + \text{c.c.} \\
&\quad + \frac{1}{2}\left(-2ik_2\frac{dA_2}{dr_2} - k_2^2A_2\right)e^{-i\mathbf{k}_2\cdot\mathbf{r}} + \text{c.c.} \\
&\quad + \omega^2\mu\epsilon_0\,[n_0^2 + (n_0n_1e^{-i\phi}e^{-i\mathbf{K}\cdot\mathbf{r}} + \text{c.c.})] \\
&\quad \times\left[\frac{A_1}{2}e^{-i\mathbf{k}_1\cdot\mathbf{r}} + \frac{A_2}{2}e^{-i\mathbf{k}_2\cdot\mathbf{r}} + \text{c.c.}\right] = 0
\end{aligned} \tag{18.1-5}$$

where we neglected

$$\frac{d^2A}{dr^2} \ll k\frac{dA}{dr}$$

We observe by inspection that spatially cumulative exchange of power takes place when the (Bragg) condition

$$\mathbf{k}_2 - \mathbf{k}_1 = \mathbf{K} \tag{18.1-6}$$

is satisfied.[1] Keeping only synchronous terms (terms with similar exponents)

[1] When condition (18.1-6) is not satisfied the power exchange reverses sign every $\Delta\ell = \pi/(|\mathbf{k}_2 - \mathbf{k}_1 - \mathbf{K}|)$. When (18.1-6) is satisfied the product term in (18.1-5) contains synchronous terms with factors $\exp(-i\mathbf{k}_1\cdot\mathbf{r})$ and $\exp(-i\mathbf{k}_2\cdot\mathbf{r})$.

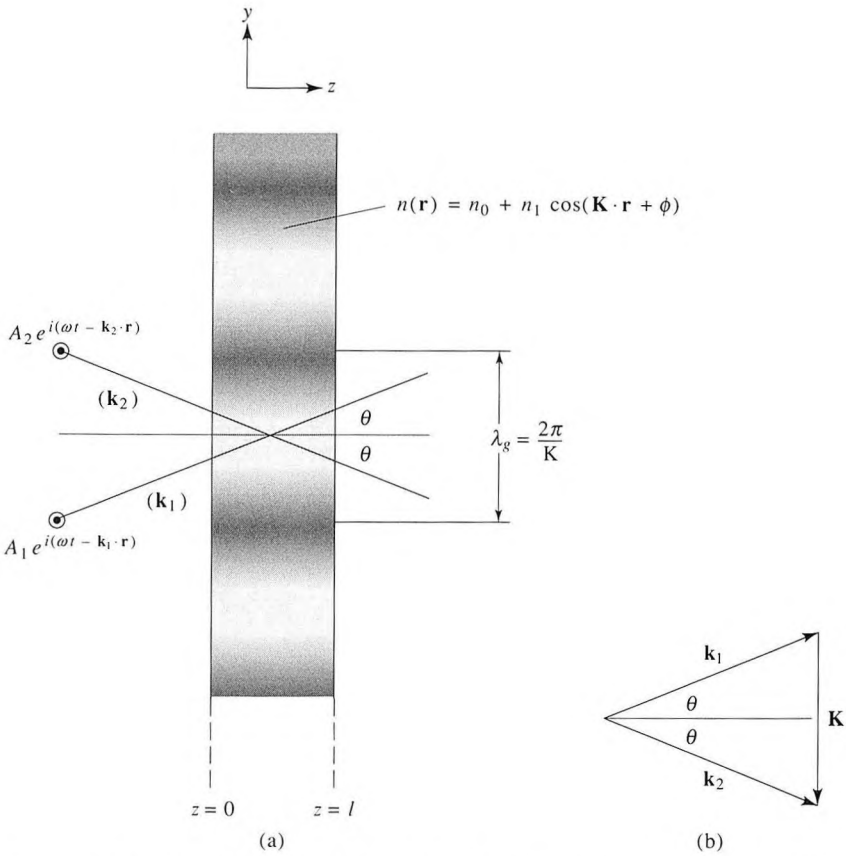

Figure 18-1 (a) Coupling between beam 1 propagating along $\mathbf{k}_1$ and beam 2 ($\mathbf{k}_2$) caused by a fixed index grating with a grating vector $\mathbf{K}$. (b) The Bragg condition diagram $\mathbf{k} = \mathbf{k}_2 - \mathbf{k}_1$.

and recalling that in an isotropic medium $k_1 = k_2 = \omega\sqrt{\mu\epsilon_0 n_0}$ helps us simplify (18.1-5)

$$\cos\theta \frac{dA_1}{dz} = -\frac{\alpha}{2} A_1 + i\frac{\pi n_1}{\lambda} e^{i\phi} A_2 e^{i(\mathbf{k}_1 - \mathbf{k}_2 + \mathbf{K})\cdot\mathbf{r}}$$

$$\cos\theta \frac{dA_2}{dz} = -\frac{\alpha}{2} A_2 + i\frac{\pi n_1}{\lambda} e^{-i\phi} A_1 e^{-i(\mathbf{k}_1 - \mathbf{k}_2 + \mathbf{K})\cdot\mathbf{r}} \qquad (18.1\text{-}7)$$

where loss terms $-(\alpha/2)\, A_{1,2}$ were added phenomenologically to account for absorption and $\lambda = 2\pi/(\omega\sqrt{\mu\epsilon_0 n_0^2})$ is the wavelength in the medium. 2θ is the angle between $\mathbf{k}_1$ and $\mathbf{k}_2$, and z is the distance measured along the bisector, so that $z = r_{1,2}\cos\theta$. Expressing the amplitudes in terms of magnitudes and phases by using the definition $A_j \equiv \sqrt{I_j}\exp(-i\phi_j)$ leads to (in what follows

we take $\mathbf{k}_1 - \mathbf{k}_2 + \mathbf{K} = 0$, i.e., the Bragg condition is satisfied)

$$\cos\theta \frac{dI_1}{dz} = -\alpha I_1 + \frac{2\pi n_1}{\lambda}\sqrt{I_1 I_2}\sin(\phi_1 - \phi_2 + \phi)$$
$$\cos\theta \frac{dI_2}{dz} = -\alpha I_2 - \frac{2\pi n_1}{\lambda}\sqrt{I_1 I_2}\sin(\phi_1 - \phi_2 + \phi) \qquad (18.1\text{-}8)$$

Note that the coupling at a point $\mathbf{r}$ depends on the local phase $\psi \equiv (\phi_1 - \phi_2 + \phi)$. If the phase ψ is zero, no power exchange takes place. If $\psi = \pm\pi/2$, the exchange is maximum. The case $\psi = \pm\pi/2$ according to Equations (18.1-1) and (18.1-2) corresponds to a grating that is displaced by a quarter period with respect to the intensity interference pattern of waves 1 and 2. In the most common scenario, a single wave, say 1, is incident on the grating and wave 2 is the diffracted wave. In this case it follows from the second equation of (18.1-7) that wave 2 is generated with a phase $\phi_2 = \phi_1 + \phi + \pi/2$, i.e. $\psi = -\pi/2$, which results, according to the second equation of (18.1-8), in a *maximum* positive value for the power exchange dI_2/dz.

The solution of (18.1-8) in the case of $\psi = -\pi/2$ becomes

$$I_1(z) = I_1(0)e^{-\alpha z}\cos^2\left(\frac{\pi n_1 z}{\lambda\cos\theta}\right)$$
$$I_2(z) = I_1(0)e^{-\alpha z}\sin^2\left(\frac{\pi n_1 z}{\lambda\cos\theta}\right) \qquad (18.1\text{-}9)$$

so that in a grating of length ℓ the diffraction efficiency is

$$\eta = \frac{I_2(\ell)}{I_1(0)} = \exp\left(-\frac{\alpha\ell}{\cos\theta}\right)\sin^2\left(\frac{\pi n_1 \ell}{\lambda\cos\theta}\right) \qquad (18.1\text{-}10)$$

This formula, first obtained by Kogelnik [1], is very useful in interpreting a large variety of experimental data involving fixed volume gratings and holograms.

We are now ready to consider the more interesting and varied case of dynamic scattering where the grating is not fixed but is generated in "real time" by the very two waves that scatter from it.

18.2 THE PHOTOREFRACTIVE EFFECT—TWO-BEAM COUPLING

In Section 18.1 we discussed the phenomenon of two-beam coupling (or diffraction) in a *fixed* hologram. In this section we will discuss the two-beam coupling by a hologram that is formed by the intensity interference pattern of the two (coupled) beams themselves. Under such circumstances the "writing" of the hologram by the two beams and the coupling of the (same) beams

by the hologram cannot be considered separately, as was done in Section 18.1, and need be treated self-consistently. The phenomenon is known variously as two-beam coupling, dynamic holography, and real-time holography. The two most important classes of interactions that give rise to two-beam coupling are stimulated Brillouin scattering and the photorefractive coupling (to be discussed in Section 18.3).

The photorefractive effect can be defined as a change in the index of refraction (n) of a material medium that is proportional to the intensity pattern of the light. It thus follows that since every material possesses a nonlinear optical response of the type given by Equation (17.3-7)

$$P_i^{(\mathrm{NL})} = 3\chi_{ijk\ell}^{(3)} E_j E_k^* E_\ell \tag{18.2-1}$$

the material also displays a photorefractive effect since for the case of a single beam, i.e., putting $i = j = k = \ell$, we can obtain from (18.2-1) the relation $\Delta n = (1/2)\,\chi^{(3)}|E|^2/(n\epsilon_0)$ where n is the index of refraction when the field amplitude is zero. The nonlinear coefficient $\chi^{(3)}$ (see Table 17-1) in most materials is very small so that one requires very large optical intensities such as are available from pulsed lasers or from guided waves in small cross-sectional optical waveguides to affect appreciable ($\Delta n > 10^{-5}$) changes of the index of refraction. The cases of stimulated Brillouin scattering and that of the photorefractive effect are an exception to the rule and lead to a very strong effects. In each of these two cases, however, the interaction is mediated by a nonlocal effect—a traveling hypersonic wave in the case of Brillouin scattering, and of a traveling, or stationary, spatially periodic charge distribution in the photorefractive case. This gives rise to index changes that are orders of magnitude larger than those due to local atomic (or molecular) nonlinear response of the type described by (18.2-1). We will start with a description of the photorefractive effect.

This effect takes place in impurity-doped electrooptic crystals (i.e., crystals lacking inversion symmetry as discussed in Section 8.1). Let such a crystal be subject to a sinusoidal intensity distribution.

$$I(x) = I_0 + I_1 e^{i(\Omega t - Kx)} + \text{c.c.} \tag{18.2-2}$$

caused by the interference of two, mutually coherent, optical beams as shown in Figure 18-2. The optical intensity causes carriers, say electrons, to be excited from occupied donor states (the N_D^0 states of Figure 18-3) to the conduction band. Once excited the now highly mobile electrons will migrate away under the influence of diffusion and any internal or external electric fields until captured by a trapping center N_D^+, usually an empty donor (i.e., a donor that has lost its outer valence electrons either by excitation to the conduction band or to a deep acceptor N_A). It follows that at steady state the high intensity regions will lose electrons while those of low intensity will acquire an excess of electrons.

The resultant space charge distribution ρ_{sc} is shown in Figure 18-2. Also shown is the electric field $E_{\mathrm{sc}} = \int \rho_{\mathrm{sc}}\, dx$ that results from the charge sepa-

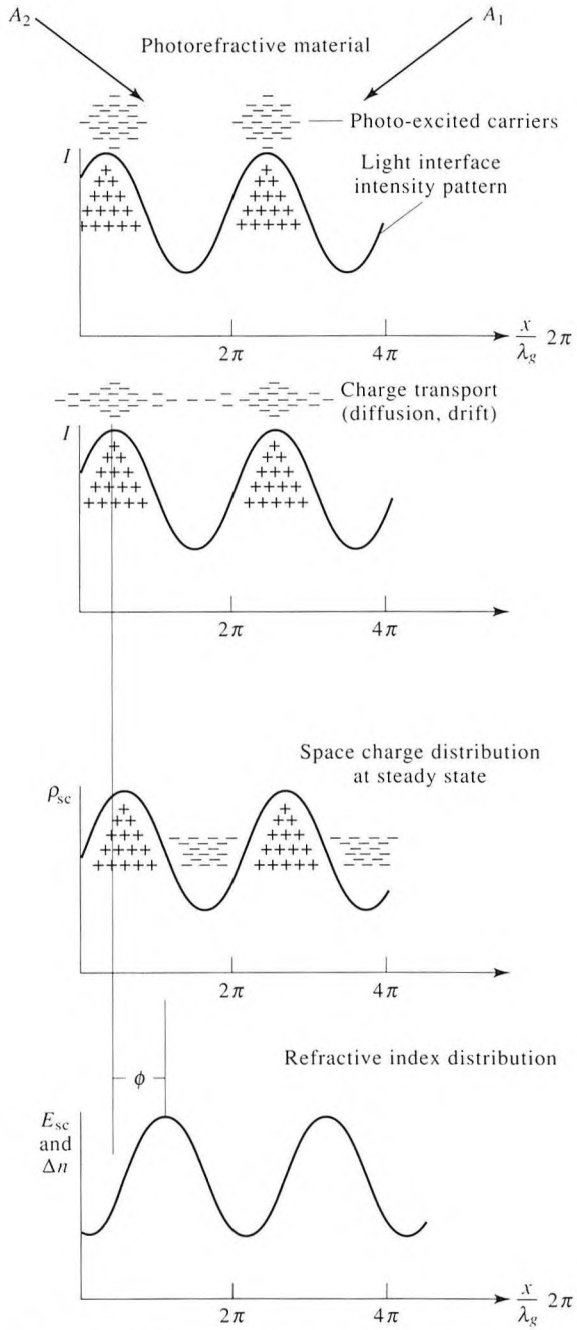

Figure 18-2 The photorefractive mechanism. Two coherent light beams intersect in an electrooptic crystal, forming an interference pattern. Electrons are excited where the intensity is large and migrate to regions of low intensity. The electric field associated with the resultant space charge operates through the electrooptic effect to produce a refractive index grating. ϕ is the phase shift (in radians) between the light interference pattern and the index grating.

ration. Since the crystal is electrooptic, an index grating $\Delta n \propto rE_{sc}$ is induced in the crystal by this field where r is the appropriate electrooptic coefficient. This index grating is displaced by a quarter period with respect to the charge distribution. This shift is due to the relation $\nabla \cdot E_{sc} = \rho_{sc}/\epsilon$. To analyze the physics of the grating formation we refer to Figure 18-3. The photorefractive crystal contains two species of atoms, the donor atoms whose density is $N_D(\text{cm}^{-3})$ and acceptor atoms (N_A). Since the energy of a valence electron in the acceptor atom state is lower than that of the donor, each acceptor atom has deprived a donor atom of an electron. This leaves behind a density $\langle N_D^+ \rangle = N_A$ of ionized donors (the $\langle\rangle$ brackets represent a spatial average). The remainder $(N_D - N_D^+)$ of the donor atoms are candidates for excitation by the optical field. Each such excitation generates a free (mobile) electron in the conduction band while, simultaneously, converting a unionized donor atom whose density is $(N_D - N_D^+)$ into an ionized N_D^+ site. Electrons can be trapped by the N_D^+ ions, returning them in the process into the unionized state. While in the conduction band the electrons are free to drift under the influence of the local electric field and diffuse.

In the above discussions we took the mobile charge carrier to be an electron. In some crystals it could be a hole. Simultaneous existence of electrons and holes is also possible. Also, the charge designation, N_D^+ and $N_D^0(=N_D - N_D^+)$, for example, is meant to represent the change in the charge state of the atom and not its true state. In some cases, $BaTiO_3$ for example, the N_D^+ state could be that of a Fe^{3+} ion, in which case N_D^0 will represent the Fe^{2+} state. This will be discussed further on in this section.

The density concentration of electrons in the conduction band is denoted by n_e. The three species listed above coexist in the presence of the interaction with the optical field as well as the diffusion, drift, and trapping processes. The process indicated in Figure 18-3 converts the donor (N_D^0) atom into an electron trap (N_D^+) while the trap, having gained an electron, becomes an N_D^0 atom so that the spatial average of each species remains constant while

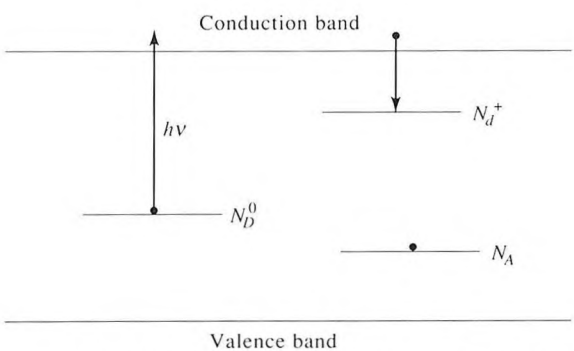

Figure 18-3 The deep impurity levels involved in the charge migration and trapping of a photorefractive crystal.

the local concentration may vary. The acceptor atoms N_A are fully occupied by electrons at all times so that in the dark $\langle N_D^+ \rangle = N_A$ where $\langle\rangle$ stands for spatial averaging. The main role of the deep acceptors N_A is to ensure that there exists everywhere a large population of traps $\langle N_D^+ \rangle \cong N_A$ that can readily capture mobile electrons. Otherwise electrons could be trapped only at the sites from which they were excited, which would not give rise to the desired charge separation (i.e., grating).

The rate equation for the donor atom density is

$$\frac{\partial N_D^+(x, t)}{\partial t} = \left(\frac{\alpha_D}{h\nu}\right) I(x)(N_D - N_D^+) - \gamma_D n_e N_D^+ \tag{18.2-3}$$

where α_D is the absorption cross section of the $N_D^0 = N_D - N_D^+$ donor state atoms. γ_D is the recombination coefficient of a free electron at an N_D^+ site. γ_D is related to the commonly used recombination cross section σ_D by $\gamma_D = \sigma_d v_{\text{th}}$ where v_{th} is the mean thermal velocity of the free electrons.

The current density $J_x(A/m^2)$ is the sum of a drift and a diffusion term

$$J_x = \mu e n_e E_x + eD \frac{\partial n_e}{\partial x} = \mu e n_e E_x + k_B T \mu \frac{\partial n_e}{\partial x} \tag{18.2-4}$$

where we use $e \equiv |e|$ and the Einstein relation $eD = k_B T \mu$ relating the electron diffusion coefficient D to the Boltzmann constant k_B, the mobility μ, and the temperature T. The current continuity relation $\nabla \cdot \mathbf{J} = -\partial\rho/\partial t$ becomes

$$\frac{\partial J_x}{\partial x} = -e \frac{\partial}{\partial t}(N_D^+ - n_e) \tag{18.2-5}$$

and the Gauss relation

$$\frac{\partial E_x}{\partial x} = \rho/\varepsilon = \frac{e(N_D^+ - n_e - N_A)}{\varepsilon} \tag{18.2-6}$$

We will first solve for $n(x, t)$, $\rho(x, t)$, and $E_x(x, t)$ by assuming that the spatial modulation is small so that it can be represented by the first two harmonics ($n = 0$, $n = 1$) of the spatial Fourier amplitudes

$$N_D^+(x, t) = D_0 + [D_1 e^{-iKx} + \text{c.c.}] \tag{18.2-7}$$

$$n_e(x, t) = n_{e0} + [n_{e1} e^{-iKx} + \text{c.c.}] \tag{18.2-8}$$

$$E_x(x, t) = E_0 + [E_1^{\text{sc}} e^{-iKx} + \text{c.c.}] \tag{18.2-9}$$

Since the crystal is charge-balanced, it follows that

$$\langle \rho \rangle = e\langle N_D^+ - n_e - N_A \rangle \equiv (D_0 - n_{e0} - N_A) = 0$$

where $\langle\rangle$ denotes averaging over x. In addition, E_0, the average value of the internal field E_x, is equal to the externally applied electric field, if one exists.

The following approximations that are justified by the actual numerical values in real crystals are made

$$\begin{array}{ccccc} N_D & \gg & N_A & \gg & n_{e0} \qquad D_1 \gg n_{e1} \\ \downarrow & & \downarrow & & \downarrow \\ \sim 10^{19}\ \text{cm}^{-3} & & \sim 10^{16}\ \text{cm}^{-3} & & 10^{13}\ \text{cm}^{-3} \end{array}$$

The electric fields of the two interfering beams are

$$\begin{aligned} \mathbf{E}_1(\mathbf{r}, t) &= \hat{\mathbf{e}}_1 A_1(\mathbf{r}) e^{i(\omega_1 t - \mathbf{k}_1 \cdot \mathbf{r})} + \text{c.c.} \\ \mathbf{E}_2(\mathbf{r}, t) &= \hat{\mathbf{e}}_2 A_2(\mathbf{r}) e^{i(\omega_2 t - \mathbf{k}_2 \cdot \mathbf{r})} + \text{c.c.} \end{aligned} \tag{18.2-10}$$

The squared magnitude of the field is thus[2]

$$\begin{aligned} I(x) &\equiv \langle (\mathbf{E}_1 + \mathbf{E}_2) \cdot (\mathbf{E}_1 + \mathbf{E}_2) \rangle_{\text{space-time}} \\ &= |A_1|^2 + |A_2|^2 + \hat{\mathbf{e}}_1 \cdot \hat{\mathbf{e}}_2 (A_1 A_2^* e^{i[(\omega_1 - \omega_2)t - (\mathbf{k}_1 - \mathbf{k}_2)\cdot \mathbf{r}]} + \text{c.c.}) \end{aligned} \tag{18.2-11}$$

Comparing the last result to (18.2-2) leads to

$$\begin{aligned} \mathbf{K} = \mathbf{k}_1 - \mathbf{k}_2 = \hat{\mathbf{e}}_x |\mathbf{k}_1 - \mathbf{k}_2| \qquad I_0 &\equiv |A_1|^2 + |A_2|^2 \\ I_1 &\equiv \hat{\mathbf{e}}_1 \cdot \hat{\mathbf{e}}_2 A_1 A_2^* \end{aligned} \tag{18.2-11a}$$

We note that the interference term I_1 is zero when the two beams are mutually orthogonal. We have also assumed that in general $\omega_1 \neq \omega_2$.

We substitute (18.2-4) into (18.2-5) and eliminate n_{e0}, E_0, n_{e1}, D_0, and D_1 using (18.2-3) and (18.2-6). We take advantage of the inequalities and neglect the product of second-order terms, and after a good deal of algebra, obtain [3]

$$E_1^{\text{sc}} = -i \frac{I_1}{I_0} \frac{E_N (E_0 + iE_D)(e^{i\Omega t} - e^{-t/\tau})}{[E_0 - \Omega t_0 (E_D + E_\mu)] + i(E_N + E_D + \Omega t_0 E_0)}$$

$$\Omega \equiv \omega_2 - \omega_1 \qquad E_N = \frac{eN_A}{\varepsilon K} \qquad E_\mu = \frac{\gamma_D N_A}{\mu K} \tag{18.2-12}$$

E_0 = externally applied field, $E_D = \dfrac{k_B T K}{e}$

$$t_0 = \frac{N_A h\nu}{\alpha_D N_D I_0} \qquad \tau = t_0 \frac{E_0 + i(E_D + E_\mu)}{E_0 + i(E_N + E_D)}$$

The steady-state response is obtained at $t \gg \tau$, at which time the transient term $\exp(-t/\tau)$ can be neglected. Under typical conditions using a grating period $2\pi K^{-1} = 2\ \mu$m and the above approximate values N_D, N_D^+, and N_A, we estimate in $BaTiO_3$

$$E_D \sim 800\ \text{V/cm} \qquad E_N \sim 118\ \text{V/cm}$$

If no applied field is present $E_0 = 0$, and the steady-state internal field (18.2-12) is

---

[2]The temporal averaging $\langle\rangle_{\text{time}}$ is over a few optical periods so that "slow" variations such as $\exp[i(\omega_1 - \omega_2)t]$ survive. The spatial averaging is over a few optical wavelengths.

$$E_1^{sc} \simeq -i\left(\frac{I_1}{I_0}\right)\frac{1}{1 + i\Omega\tau}\frac{E_D}{(1 + E_D/E_N)}$$

$$\tau = t_0\frac{1 + E_\mu/E_D}{1 + E_N/E_D} \tag{18.2-13}$$

If we take the steady-state limit of Equation (18.2-12) in the case $\omega_1 = \omega_2$ ($\Omega = 0$) and no external field ($E_0 = 0$), we obtain

$$E_1^{sc} \approx -i\frac{I_1}{I_0}\frac{E_D}{1 + \dfrac{E_D}{E_N}} \tag{18.2-14}$$

A few basic features of fundamental importance for practical applications stand out:

1. The factor $(-i)$ represents a quarter period shift of the index grating with respect to the intensity pattern.
2. E_1^{sc} (and Δn) depend not on the total intensity but on the fractional modulation I_1/I_0.
3. The space charge field tends toward the smaller of the E_N and E_d (multiplied by I_1/I_0).

These last two conclusions merit some further discussion: The total amount of separable charge is limited. The maximum separation would result when approximately *all* the traps in the low intensity regions are full, while all the traps in the high intensity regions are emptied. Since the initial density of such traps is $N_D^+ = N_A$, the resulting charge density can be approximated by

$$\rho_{sc} = N_A e \cos Kx = Re(N_A e e^{iKx})$$

From the Gauss law $\nabla \cdot \mathbf{E} = \rho/\epsilon$, we obtain, using complex notation,

$$E_1^{sc} = -\frac{ieN_A}{\epsilon K} = -iE_N \tag{18.2-15}$$

We thus identify E_N with the *maximum* space charge field that results from *full separation* (by half the grating period $\lambda/2 = \pi/K$) of the available charge (eN_A per unit volume).

The question then arises as to why the internal field is prevented from reaching a value $\sim E_N$ and is limited, instead, to a value of $\sim E_D = k_B TK/e$ when $E_N > E_d$. To answer this question, consider the electron current resulting from the excitation of some initial distribution of mobile carriers into the conduction band in the *presence* of a space charge field E_1^{sc} (due to earlier charge separation). From (18.2-4)

$$J_e = \mu e n_e E_1^{sc} + k_B T\mu\frac{\partial n_e}{\partial x} \qquad (\mu,\ e < 0 \text{ for electrons})$$

Since the initial distribution n_e mimics the (negative) of the intensity (18.2-2), we can write

$$n_e(x) = n_{e0} - (n_{e1}e^{-iKx} + \text{c.c.}) \qquad \text{and}$$
$$E_{sc}(x) = E_1^{sc}e^{-iKx} + \text{c.c.}$$

The fundamental component of the current density becomes

$$J_e = (\mu e n_{e0}E_1^{sc} + iKk_BT\mu n_{e1})e^{-iKx} + \text{c.c.}$$

It follows that the electron current vanishes when the space charge field E_1^{sc} reaches a value

$$E_1^{sc} = -i\frac{k_BTK}{e}\left(\frac{n_{e1}}{n_{e0}}\right) \equiv -iE_D\left(\frac{n_{e1}}{n_{e0}}\right)$$

and no further charge separation takes place. The internal space periodic field E_1^{sc} thus gets arrested at a value $\sim E_D$ and cannot achieve the charge-limited value of E_N. This situation changes in the presence of an external field E_0 that can "overpower" the internal space charge field so that E_1^{sc} tends, according to (18.2-12), to a value of $\sim -i(I_i/I_0)E_N$, corresponding to full charge separation. Figure 18-4 shows the theoretical dependence of the space charge field E_1^{sc} on the external field E_0. Of special interest is the change of E_1^{sc} from an initial value smaller than the smallest of E_N and E_D

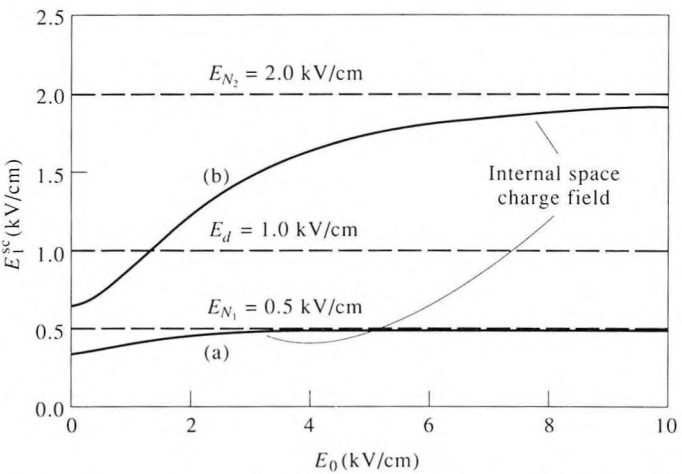

Figure 18-4 A theoretical plot of the amplitude E_1^{sc} of the spatially periodic internal electric field in photorefractive crystals [see Equation (18.2-12)] with $\Omega = 0$, $t \to \infty$ as a function of the externally applied field E_0. The characteristic fields are: $E_D = 10^3$ V/cm and (a) $E_N = 5 \times 10^2$ V/cm, (b) $E_N = 2 \times 10^3$ V/cm. (Private communication K. Sayano, The California Institute of Technology and R. R. Neurgaonkar, Rockwell International Corp.)

to a final value approaching E_N. In this particular example a large trap concentration N_A leading to a limiting field of $E_{N2} = 2 \times 10^3$ V/cm should give, according to curve (b), a fourfold increase in the internal space charge field with the application of an external field $E_0 \sim 10^4$ V/cm. Figure 18-5 shows experimental data from two strontium barium niobate $Sr_xBa_{1-x}Nb_2O_6$ (SBN:x = 60%) crystals doped with Cr. An increase in the space charge field by about a factor of three is seen for $E_0 \sim 10^4$ V/cm. Experimental data of the dependence of E_1^{sc} on E_0 is shown in Figure 18-5. The values of E_1^{sc} are deduced from two-beam coupling experiments that are discussed later.

Two of the most important features of the analysis are the dependence of the internal field E_1^{sc} on the grating period λ_g and the dependence of τ on intensity [6]. If we use the above definitions of E_D and E_N, we can rewrite E_1^{sc} of (18.2-12) as

$$E_1^{sc} = -i\left(\frac{I_1}{I_0}\right)\left(\frac{1}{1 + i\Omega\tau}\right)\frac{(k_BTK/e)}{1 + \dfrac{\varepsilon k_BTK^2}{e^2N_A}} \tag{18.2-16}$$

so that the limits of $K \to 0$ ($\lambda_g \to \infty$) and $K \to \infty$ ($\lambda_g \to 0$), $E_1^{sc} \to 0$. Experimental evidence illustrating the dependence of E_1 on the grating period is shown in Figure 18-6, which shows an experimental plot of a quantity proportional to the internal field as a function of the grating period $\lambda_g = 2\pi K^{-1}$. Figure 18-7 shows the measured dependence of τ on the intensity I_0.

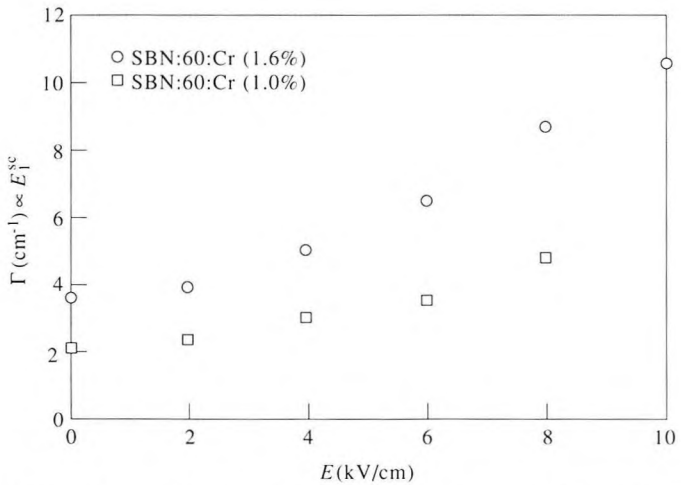

Figure 18-5 Experimental data of the two-beam coupling gain $\Gamma \propto E_1^{sc}$ as a function of applied electric field E_0 in two doped SBN:60 crystals. (After Reference [4].)

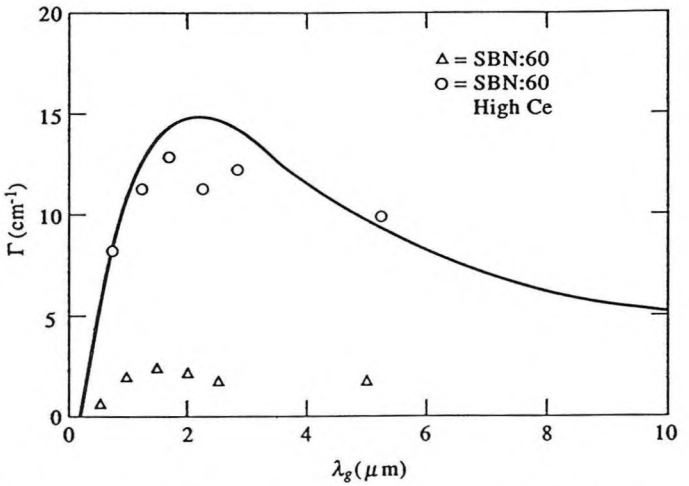

Figure 18-6 Two-beam coupling coefficient versus grating wavelength for $E_0 = 0$. The coupling coefficient Γ is proportional to the internal field E_1^{sc} of Equation (18.2-16). (After Reference [5].)

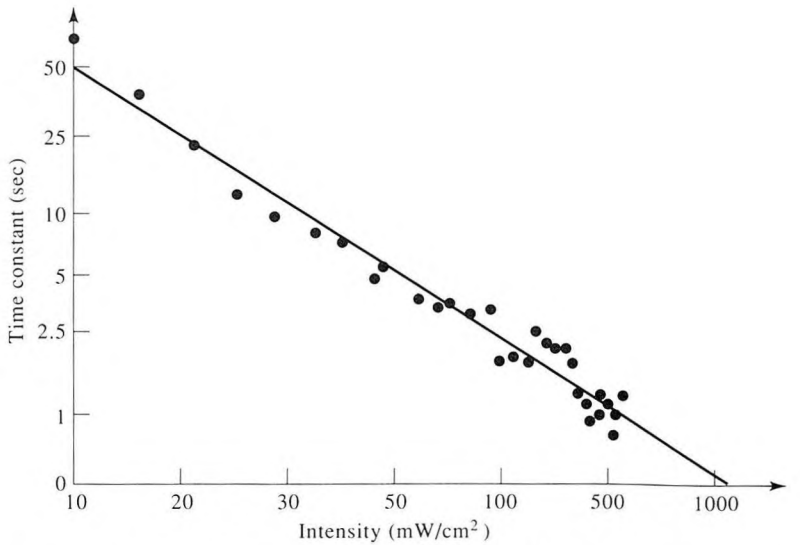

Figure 18-7 Photorefractive response time of the $BaTiO_3$ crystal versus intensity for $\lambda = .605\ \mu m$, $\lambda_g = 1.4\ \mu m$. (After Reference [5].)

The Grating Formation

Now that we have determined the space-periodic electric field created by two interfering optical beams (18.2-12), we will derive an expression for the resulting refractive index grating induced by this field.

The change in the optical indicatrix due to a (low frequency) electric field E_k is given according to (9.2-1) by

$$\Delta\left(\frac{1}{n^2}\right)_{ij} = r_{ijk}E_k$$

where r_{ijk} is the electrooptic tensor element. This corresponds to a change in the index of refraction experienced by a propagating wave

$$\Delta n \equiv -\frac{1}{2}\, n_0^3 r_{\text{eff}} E \tag{18.2-17a}$$

where E is the low-frequency electric field, and r_{eff} is some linear combination of the electrooptic tensor elements r_{ijk} that depends on the crystal orientation and the field direction. We describe the spatial dependence of the index of refraction as

$$n(x, t) \equiv n_0 + \frac{1}{2}\left[\frac{n_1 e^{-i\phi} I_1}{I_0}\, e^{i(\Omega t - Kx)} + \text{c.c.}\right] \tag{18.2-17b}$$

where $I_0 = |A_1|^2 + |A_2|^2$, $I_1 = \hat{\mathbf{e}}_1 \cdot \hat{\mathbf{e}}_2 A_1 A_2^*$ so that, using (18.2-17a), n_1 is defined by

$$\frac{n_1 e^{-i\phi} I_1}{I_0} = \frac{n_1 e^{-i\phi} \hat{\mathbf{e}}_1 \cdot \hat{\mathbf{e}}_2 A_1 A_2^*}{I_0} = -n_0^3 r_{\text{eff}} E_1^{\text{sc}} \tag{18.2-18}$$

We take n_1 as real so that ϕ is the phase shift between the intensity pattern and that of the index $n(x)$. The quantity n_1 is thus the index modulation amplitude (within a factor I_1/I_0). From (18.2-13) in the case $\omega_1 = \omega_2$ ($\Omega = 0$)

$$n_1 e^{-i\phi} \simeq r_{\text{eff}} n_0^3 \frac{iE_N(E_0 + iE_D)}{E_0 + i(E_N + E_D)} \tag{18.2-19}$$

We note from (18.2-17) and (18.2-19) that the index modulation does not depend on the absolute intensity but only on the spatial modulation index $I_1/I_0 \equiv |\hat{\mathbf{e}}_1 \cdot \hat{\mathbf{e}}_2 A_1 A_2^*|/I_0$. This reflects the fact that the role of the optical field is only to redistribute the electronic charge so that the maximum space charge field and Δn are limited, as discussed above, only by diffusion processes and by the total available charge, but not by the intensity.

Refractive Two-Beam Coupling The index grating registered by beams E_1 and E_2 in a photorefractive medium causes power transfer by coupling E_1 and E_2 to each other. The coupling is due to simultaneous Bragg scattering of both beams from the grating into each other. Since the grating is due to

the interference of the two beams, the Bragg condition $\mathbf{K} = \mathbf{k}_1 - \mathbf{k}_2$ is automatically satisfied and ensures that beam 1 is diffracted exactly in the direction of beam 2 and vice versa, hence the coupling between the two beams. What's more, in the case where $\omega_1 \neq \omega_2$, the grating moves with just the right velocity $((\omega_2 - \omega_1)/K)$ so that the Doppler-shifted frequency of the incident beam 1, i.e., $\omega_1 + \Delta\omega_{\text{Doppler}}$, is equal to that of beam 2 (ω_2) and vice versa. The analysis starts with the wave equation (6.5-3).

$$\nabla^2\mathbf{E} + \omega^2\mu\varepsilon(\mathbf{r})\mathbf{E} = 0, \qquad \varepsilon(\mathbf{r}) = \varepsilon_0 n^2(\mathbf{r}) \tag{18.2-20}$$

Using Equation (18.2-18) for $n(\mathbf{r})$, assuming $n_1 \ll n_0$, and putting $\omega^2\mu\varepsilon_0 = \omega^2/c^2$ lead to

$$\nabla^2\mathbf{E} + \frac{\omega^2}{c^2}\left[n_0^2 + \frac{n_0 n_1 e^{-i\phi}\hat{\mathbf{e}}_1 \cdot \hat{\mathbf{e}}_2 A_1 A_2^*}{I_0}\, e^{i(\Omega t - Kx)} + \text{c.c.}\right]\mathbf{E} = 0 \tag{18.2-21}$$

The field $\mathbf{E}$ is the sum of the two fields $\mathbf{E}_1$ and $\mathbf{E}_2$ (18.2-10) that "write" the grating. If we substitute $\mathbf{E}$ into (18.2-21) and for simplicity replace the vector $\mathbf{E}$ by a scalar E [this requires the use of the proper electrooptic coefficient, or combination of coefficients, r_{eff} in (18.2-18)], the result is

$$\begin{aligned}
&\left[-2ik_1\frac{dA_1}{dr_1} - \frac{d^2}{dr_1^2}A_1(r_1) - k_1^2 A_1(r_1)e^{i(\omega_1 t - k_1 r_1)} + \text{c.c.}\right] \\
&+\left[-2ik_2\frac{dA_2}{dr_2} - \frac{d^2}{dr_2^2}A_2(r_2) - k_2^2 A_2(r_2)e^{i(\omega_2 t - k_2 r_2)} + \text{c.c.}\right] \\
&+\frac{\omega^2}{c^2}\left[n_0^2 + (n_0 n_1 e^{-i\phi}\frac{\hat{\mathbf{e}}_1 \cdot \hat{\mathbf{e}}_2 A_1 A_2^*}{I_0}\, e^{i[(\omega_1-\omega_2)t - (k_1 r_1 - k_2 r_2)]} + \text{c.c.}\right] \\
&\times [A_1(r_1)\varepsilon^{i(\omega_1 t - k_1 r_1)} + A_2(r_2)e^{i(\omega_2 t - k_2 r_2)} + \text{c.c.}] = 0
\end{aligned} \tag{18.2-22}$$

Recognizing that $k_{1,2} = \dfrac{\omega_{1,2} n_0}{c}$, neglecting the second derivative terms compared to those involved in the first derivatives (this is the slowly varying amplitude approximation), and equating separately terms with the same exponential factors lead to the coupled wave equations

$$\begin{aligned}
\cos\theta_1 \frac{dA_1}{dz} &= -\frac{\alpha}{2}A_1 + i\frac{\pi n_1}{\lambda}e^{-i\phi}\frac{|A_2|^2}{I_0}\hat{\mathbf{e}}_1 \cdot \hat{\mathbf{e}}_2 A_1 \\
\cos\theta_2 \frac{dA_2}{dz} &= -\frac{\alpha}{2}A_2 + i\frac{\pi n_1^*}{\lambda}e^{+i\phi}\frac{|A_1|^2}{I_0}\hat{\mathbf{e}}_1 \cdot \hat{\mathbf{e}}_2 A_2
\end{aligned} \tag{18.2-23}$$

where θ_1 and θ_2 are the angles between $\mathbf{k}_1$ and $\mathbf{k}_2$ and the normal to the crystal input face, taken as $z = 0$. The loss term α was added phenomenologically to account for absorption in the crystal.

Before considering some exact consequences of (18.2-23), we might contemplate some qualitative features. Using (18.2-19) in the limit $E_N \gg E_D$, $E_0 = 0$ and $\phi = \pi/2$, we can recast (18.2-23) in the form of

$$\cos\theta_1 \frac{dA_1}{dz} = -\frac{\alpha}{2} A_1 - \left[\frac{\pi n_0^3}{\lambda} r_{\text{eff}}(\hat{\mathbf{e}}_1 \cdot \hat{\mathbf{e}}_2) \frac{E_D|A_2|^2}{I_0}\right] A_1$$

$$\cos\theta_2 \frac{dA_2}{dz} = -\frac{\alpha}{2} A_2 + \left[\frac{\pi n_0^3}{\lambda} r_{\text{eff}}(\hat{\mathbf{e}}_1 \cdot \hat{\mathbf{e}}_2) \frac{E_D|A_1|^2}{I_0}\right] A_2 \qquad (18.2\text{-}24)$$

which for $r_{\text{eff}} > 0$ indicates the growth of A_2 at the expense of A_1 with an initial exponential growth constant

$$\gamma = \left[\frac{\pi n_0^3}{\lambda} r_{\text{eff}}(\hat{\mathbf{e}}_1 \cdot \hat{\mathbf{e}}_2) E_D \frac{|A_1|^2}{I_0} - \frac{\alpha}{2}\right] \qquad (18.2\text{-}25)$$

The direction of power flow depends on the sign of r_{eff} and thus can be reversed by inverting the crystal orientation. Defining normalized intensities as $\mathcal{J}_1 = |A_1|^2$, $\mathcal{J}_2 = |A_2|^2$, we obtain directly from (18.2-23)

$$\cos\theta_1 \frac{d\mathcal{J}_1}{dz} = -\alpha\mathcal{J}_1 - \frac{2\pi n_1}{\lambda} \hat{\mathbf{e}}_1 \cdot \hat{\mathbf{e}}_2 \sin(\phi)\mathcal{J}_1\mathcal{J}_2$$

$$\cos\theta_2 \frac{d\mathcal{J}_2}{dz} = -\alpha\mathcal{J}_2 + \frac{2\pi n_1}{\lambda} \hat{\mathbf{e}}_1 \cdot \hat{\mathbf{e}}_2 \sin(\phi)\mathcal{J}_1\mathcal{J}_2 \qquad (18.2\text{-}26)$$

A similar analysis for ordinary nonlinear transparent materials that are characterized by a real $\chi^{(3)}$ will lead to $\phi = 0$ ($I(x)$ and $n(x)$ "in step") so that, according to (8.2-26), no power exchange takes place. In a photorefractive material, on the other hand, where $n(x)$ is given by Equation (18.2-17, 18.2-19), $\phi = \pm\pi/2$ is possible and the power transfer is maximum. By adding the last two equations, we obtain

$$\frac{d}{dz}(\mathcal{J}_1 \cos\theta_1 + \mathcal{J}_2 \cos\theta_2) = -\alpha(\mathcal{J}_1 + \mathcal{J}_2)$$

which in the case of $\alpha = 0$ amounts to conservation of total power.

Two-Beam Coupling—Symmetric Geometry

In the case of $\theta_1 = -\theta_2 \equiv \theta$, illustrated in Figure 18.8, Equation (18.2-26) can be solved exactly. If we define $J_{1,2} \equiv \mathcal{J}_{1,2}e^{\alpha r}$, $r_1 = r_2 \equiv r = z/\cos\theta$ is the distance measured along the beams' propagation directions

$$\frac{dJ_1}{dr} = -2\Gamma \frac{J_1J_2}{J_t} = -2\Gamma \frac{J_1(J_t - J_1)}{J_t}$$

$$\frac{dJ_2}{dr} = 2\Gamma \frac{J_1J_2}{J_t} = 2\Gamma \frac{J_2(J_t - J_2)}{J_t} \qquad (18.2\text{-}27)$$

$$J_t \equiv J_1 + J_2$$

$$2\Gamma = \frac{2\pi n_1}{\lambda} \hat{\mathbf{e}}_1 \cdot \hat{\mathbf{e}}_2 \sin\phi \qquad (18.2\text{-}28)$$

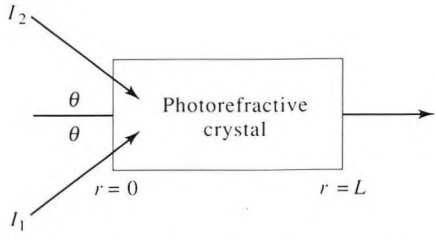

Figure 18-8 The symmetric two-beam coupling configuration.

These equations can be integrated directly. The result, when expressed in terms of the original intensity variables, is

$$\mathcal{I}_1(r) = \mathcal{I}_1(O)e^{-\alpha r}\frac{\mathcal{I}_1(O) + \mathcal{I}_2(O)}{\mathcal{I}_1(O) + \mathcal{I}_2(O)e^{2\Gamma r}}$$

$$\mathcal{I}_2(r) = \mathcal{I}_2(O)e^{-\alpha r}\frac{\mathcal{I}_1(O) + \mathcal{I}_2(O)}{\mathcal{I}_1(O)e^{-2\Gamma r} + \mathcal{I}_2(O)} \qquad (18.2\text{-}29)$$

In the case of $\mathcal{I}_2(O) \ll \mathcal{I}_1(O)e^{-2\Gamma r}$, the last equation becomes

$$\mathcal{I}_2(r) = \mathcal{I}_2(O)e^{(2\Gamma-\alpha)r} \qquad (18.2\text{-}30)$$

This predicted power exchange has been observed first by Staebler and Amodei in 1972 (Reference [7]).

Numerical Example: Two-Beam Coupling in $BaTiO_3$

$BaTiO_3$ is an electrooptic crystal with a perovskite structure that is ferroelectric at room temperature (its electrooptic constants are listed in Table 9-2), which possesses an extremely large electrooptic coefficient. The particular coefficient that comes into play in the two-beam coupling is $r_{51} = r_{42} = 16.4 \times 10^{-10}$ m/V. Using the following data $n_0 = 2.5$, $r_{\text{eff}} \approx r_{42}/2$, $E_1^{\text{sc}} \sim E_D \simeq 5 \times 10^2$ V/cm, $\lambda = 0.5\ \mu$m, $\phi = \pi/2$, $\hat{\mathbf{e}}_1 = \hat{\mathbf{e}}_2$. $\alpha = 0$, $I_1 = I_2 = I_0/2$, and using Equations (18.2-28) and (18.2-18)

$$2\Gamma = \frac{2\pi n_1}{\lambda}\sin\phi \approx \frac{\pi}{\lambda}n_0^3 r_{\text{eff}}E_D \approx 40\ \text{cm}^{-1}$$

This is a very large gain constant. To put it in perspective we may recall that most laser media provide gain of good deal less than 1 cm^{-1}. As a matter of fact, only in semiconductor lasers do we encounter similar gains.

The analogy of photorefractively induced gain to ordinary laser gain is quite fundamental since in the presence of gain all we need do to obtain

oscillation is to provide optical feedback. A whole new class of optical devices has sprung over the last few years that depends on photorefractively pumped oscillators [11, 12]. Some of these devices will be described in the remainder of this chapter. Reference [15] contains a number of review articles on photorefractive topics.

18.3 PHOTOREFRACTIVELY PUMPED OSCILLATORS AND SELF-PUMPED PHASE CONJUGATION (advanced topic)

The large optical amplification by two-beam coupling in photorefractive crystals can be used to "pump" a new class of optical oscillators, and these in turn can perform a variety of tasks. Most of these tasks involve passive phase-conjugate reflectors, that is, phase-conjugating mirrors that do not require externally supplied pump beams [9, 10]. To illustrate this principle, consider the configuration of Figure 18-9.

An input beam 4 provides gain, by two-beam coupling, to beam 1 in a photorefractive crystal placed inside a two-mirror (R_1, R_2) optical resonator. If this gain is sufficient to overcome the crystal and mirror losses, an oscillating optical field builds up inside the resonator. The two traveling beams 1 and 2 that make up the oscillating field then play the role of the conventional pump beams as in the canonical four-wave phase-conjugation geometry of Figure 17-2, resulting in a reflected beam 3 that is the phase-conjugate replica of the input beam 4.

The possibility of phase conjugation without externally provided pump beams, the so-called "self-phase conjugation," opens up a new area of practical applications involving image processing and distortion correction. Before we move on to discuss these applications, we show in Figure 18-10 an impressive demonstration of correction for propagation distortion following passive (self-pumped) phase conjugation by J. Feinberg [10]. The feedback for the photorefractive oscillation in this case is provided not by external reflectors, as in Figure 18-9, but by total internal reflection in the

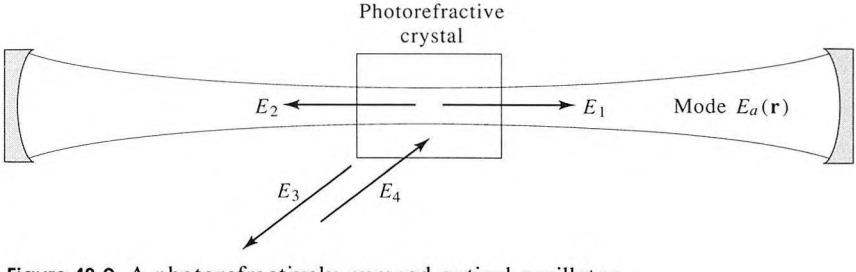

Figure 18-9 A photorefractively pumped optical oscillator.

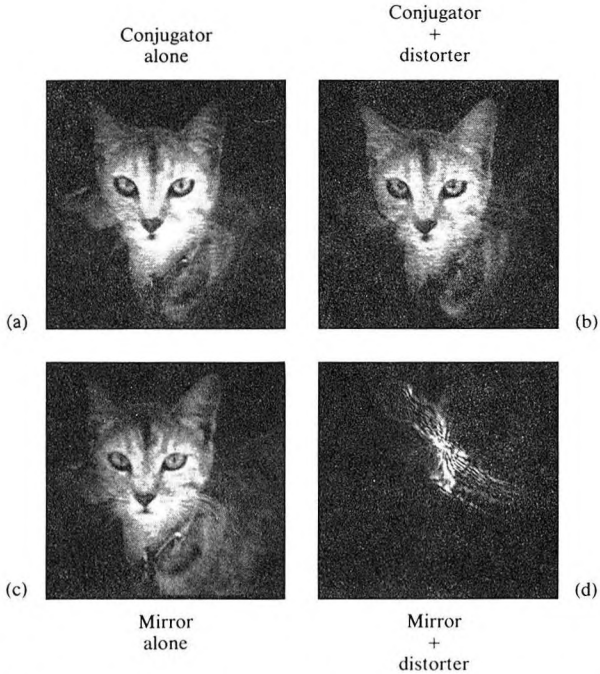

Figure 18-10 Images of a cat reflected from a self-pumped phase conjugate mirror (SPPCM) of $BaTiO_3$, a combination of a distorter and a SPPCM, an ordinary mirror, and an ordinary mirror plus a distorter. (Courtesy of J. Feinberg, University of Southern California [10].)

photorefractive ($BaTiO_3$ crystals). The point to appreciate here is the comparison of the distorted image (image + distorter) to the distorted and (phase) conjugated image (conjugator + distorter).

To analyze the general case of oscillation in a photorefractive medium [11, 12] we refer to the model of Figure 18-11. Our basic method of analysis will be to assume an oscillating mode "a" inside the resonator and find the polarization set up inside the photorefractive crystal due to the interaction of field a and the input field. We shall then insist self-consistently that the resonator mode that is excited by this polarization is the same mode a assumed at the outset. We take the known input field as

$$\mathbf{E}_i(\mathbf{r}, t) = \tfrac{1}{2}\,\mathbf{E}_{i0}(\mathbf{r})\exp(i\omega_0 t) + \text{c.c.} \qquad (18.3\text{-}1)$$

where $\mathbf{E}_{i0}(\mathbf{r})$ contains the propagation factor as well as describing the effect of distortion and of information (spatial) modulation of the beam. The oscillating beam, which establishes itself in the ring oscillator, is taken as $\mathbf{E}(\mathbf{r}, t)$, and our immediate task is to solve for the oscillation condition and

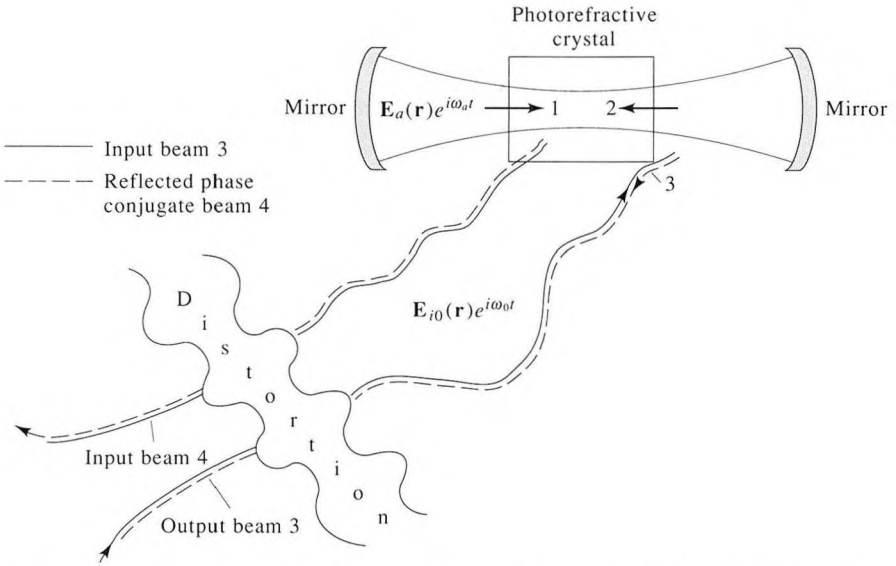

Figure 18-11 A distorted optical beam, i.e., a beam with a complicated wavefront, reflecting its propagation history, of frequency ω_0 and spatial mode profile $E_i(\mathbf{r})$ is incident on an optical resonator that can support spatial modes $E_a(\mathbf{r})$.

the oscillation frequency of this beam. The resonator field can be expanded in the (complete) set of the resonator modes $E_a(r)$ [13, 14].

$$\mathbf{E}(\mathbf{r}, t) = \sum_a -\frac{1}{\sqrt{\epsilon}} p_a(t)\mathbf{E}_a(\mathbf{r})$$

$$\mathbf{H}(\mathbf{r}, t) = \sum_a \frac{1}{\sqrt{\mu}} \omega_a q_a(t)\mathbf{H}_a(\mathbf{r}) \qquad (18.3\text{-}2)$$

where $\mathbf{E}_a(\mathbf{r})$ and $\mathbf{H}_a(\mathbf{r})$ are the spatial mode functions for the electric and magnetic fields. ϵ and μ are electric and magnetic permittivities, respectively. In addition,

$$\nabla \times \mathbf{E}_a = k_a \mathbf{H}_a$$

$$\nabla \times \mathbf{H}_a = k_a \mathbf{E}_a \qquad (18.3\text{-}3)$$

where $k_a = \omega_a\sqrt{\omega\varepsilon}$. The quantity $p_a(t)$, for example, contains the temporal information of mode a, including that of the frequency. In addition, the modal functions $\mathbf{E}_a$ and $\mathbf{H}_a$ are orthonormal

$$\int_{V_{\text{res}}} \mathbf{E}_a \cdot \mathbf{E}_b dV = \delta_{\text{ab}} \qquad \int_{V_{\text{res}}} \mathbf{H}_a \cdot \mathbf{H}_b dV = \delta_{ab}$$

The resonator contains a distributed polarization field $\mathbf{P}_{\text{NL}}(\mathbf{r}, t)$, to be specified later, due to the photorefractive two-beam coupling so that Maxwell's

equations can be written as

$$\nabla \times \mathbf{H} = \mathbf{i} + \frac{\partial}{\partial t}(\epsilon_0 \mathbf{E} + \mathbf{P}_{\text{nonresonant}} + \mathbf{P}_{\text{NL}})$$

$$= \sigma \mathbf{E} + \epsilon \frac{\partial \mathbf{E}}{\partial t} + \frac{\partial}{\partial t}\mathbf{P}_{\text{NL}}$$

$$\nabla \times \mathbf{E} = -\mu \frac{\partial \mathbf{H}}{\partial t} \tag{18.3-4}$$

σ is the effective conductivity that is introduced to account for the losses. If we use (18.3-2) and (18.3-3), (18.3-4) becomes

$$\sum_a \frac{1}{\sqrt{\mu}} \omega_a q_a k_a \mathbf{E}_a = -\sigma \sum_a \frac{1}{\sqrt{\epsilon}} p_a \mathbf{E}_a - \sum_a \sqrt{\epsilon} \dot{p}_a \mathbf{E}_a + \frac{\partial}{\partial t}\mathbf{P}_{\text{NL}}(\mathbf{r}, t) \tag{18.3-5}$$

Taking the scalar product of (18.3-5) and $\mathbf{E}_1$, integrating over the resonator volume, and using the orthonormality condition (17.3-4) leads to

$$\omega_1^2 q_1 + \frac{\sigma}{\epsilon} p_1 + \dot{p}_1 - \frac{1}{\sqrt{\epsilon}} \frac{\partial}{\partial t} \int_v \mathbf{P}_{\text{NL}} \cdot \mathbf{E}_1 \, dV = 0 \tag{18.3-6}$$

$$\omega_1^2 \dot{q}_1 + \frac{\sigma}{\epsilon} \dot{p}_1 + \ddot{p}_1 - \frac{1}{\sqrt{\epsilon}} \frac{\partial^2}{\partial t^2} \int_v \mathbf{P}_{\text{NL}} \cdot \mathbf{E}_1 \, dV = 0 \tag{18.3-7}$$

From (18.3-2), the second equation in (18.3-3), and (18.3-4) we obtain

$$p_\ell = \dot{q}_\ell$$

so that (18.3-7) becomes

$$\omega_1^2 p_1 + \ddot{p}_1 + \frac{\omega_1}{Q_1} \dot{p}_1 = \frac{1}{\sqrt{\epsilon}} \frac{\partial^2}{\partial t^2} \int_v \mathbf{P}_{\text{NL}}(\mathbf{r}, t) \cdot \mathbf{E}_1(\mathbf{r}) \, dV \tag{18.3-8}$$

where in accordance with (4.7-5) we replaced σ/ϵ by ω_1/Q_1. Q_1 is the quality factor of the resonator for mode 1. From Equation (18.3-8) we identify ω_1 as the resonance frequency of a mode 1 in the no-loss ($Q_1 \to \infty$) limit. The distributed nonlinear polarization term $\mathbf{P}_{\text{NL}}(\mathbf{r}, t)$ driving the oscillation of the resonator field is that produced by the incidence of the input field $\mathbf{E}_i(\mathbf{r}, t)$ on the index grating created photorefractively by the interaction of the field $\mathbf{E}_i(\mathbf{r}, t)$ and the ring-oscillator field $\mathbf{E}_1(r, t)$.

The nonlinear polarization P_{NL} is given by

$$\mathbf{P}_{\text{NL}}(\mathbf{r}, t) = 4\epsilon_0 \Delta n(\mathbf{r}, \mathbf{t}) \mathbf{E}_i(\mathbf{r}, t) \tag{18.3-9}$$

Referring to the derivation of the index grating equations (18.2-17, 18.2-18, 18.2-19), we identify

$$\hat{\mathbf{e}}_2 A_2(\mathbf{r}) e^{i\omega_2 t} \longrightarrow E_{i0}(\mathbf{r}) e^{i\omega_0 t}$$

$$\hat{\mathbf{e}}_1 A_1(\mathbf{r}) e^{i\omega_1 t} \longrightarrow \frac{1}{\sqrt{\epsilon}} p_1(t) \mathbf{E}_1(\mathbf{r}) \tag{18.3-10}$$

$$I_0 \equiv |A_1|^2 + |A_2|^2 \longrightarrow |E_{i0}^*|^2 + (1/\epsilon)|p_1 E_1(r)|^2$$

$$I_1 \equiv \hat{\mathbf{e}}_1 \cdot \hat{\mathbf{e}}_2 A_1 A_2^* \exp[i(\omega_1 - \omega_2)t] \longrightarrow \left(\frac{1}{\sqrt{\epsilon}}\right)\mathbf{E}_{i0}(\mathbf{r}) \cdot \mathbf{E}_1(\mathbf{r}) p_1(t) e^{-i\omega_0 t}$$

The grating equations (18.2-17, 18.2-18) thus lead to

$$\Delta n(\mathbf{r}, t) = \frac{1}{2}\frac{n_1 e^{-i\phi} I_1}{I_0} e^{-i(\Omega t - Kx)} + \text{c.c.}$$

$$\longrightarrow -\frac{\gamma p_1(t)[\mathbf{E}_{i0}(\mathbf{r}) \cdot \mathbf{E}_1(\mathbf{r})] e^{i\omega_0 t}}{2\sqrt{\epsilon}\left[|E_{i0}(\mathbf{r})|^2 + \frac{1}{\epsilon}|p_1(t)E_1|^2\right]} + \text{c.c.} \qquad (18.3\text{-}11)$$

where from (18.2-17, 18.2-18) and (18.2-12)

$$\gamma \equiv i\frac{r_{\text{eff}} n_0^3 E_N (E_0 + iE_D)}{2[E_0 - (\omega - \omega_0)t_0(E_D + E_\mu)] + i[E_N + E_D + (\omega - \omega_0)t_0 E_0]} \qquad (18.3\text{-}12)$$

ω and ω_0, we recall, are the frequency (as yet unknown) of the oscillating mode 1 and that of the pump beam, respectively. If there is no applied electric field $E_0 = 0$, we can express γ in the form

$$\gamma = \frac{i\gamma_0}{1 + i(\omega - \omega_0)\tau} \qquad (18.3\text{-}13)$$

where

$$\gamma_0 = \frac{r_{\text{eff}} n_0^3}{2}\frac{E_N E_d}{(E_N + E_d)}$$

and

$$\tau = t_0\left(\frac{E_d + E_\mu}{E_d + E_N}\right)$$

We note that the sole time dependence of $\mathbf{P}_{\text{NL}}(\mathbf{r}, t)$ is that of a mode 1, i.e., of the term $p_1(t)$. The time dependence of the input mode $\mathbf{E}_i(\mathbf{r}, t)$ has disappeared since $\mathbf{E}_i$ appears in Equation (18.3-9) multiplied by its complex conjugate. An equivalent way to explain this fact is that the index grating produced by the interference of $\mathbf{E}_i$ and $\mathbf{E}_1$ (the cavity field) is moving since $\omega \neq \omega_0$ and this velocity is just the right one to Doppler shift the incident frequency ω_0 to that of the oscillating mode ω.

Returning to the oscillation equation (18.3-8), we take $p_1(t)$ as the product of a slowly varying amplitude $p_{10}(t)$ and an optical oscillation term $\exp(i\omega t)$:

$$p_1(t) = p_{10}(t)e^{i\omega t}$$

In addition, we use Equation (18.3-9) to obtain in the process

$$\left\{\left[(\omega_1^2 - \omega^2) + i\frac{\omega_1\omega}{Q_1}\right]p_{10}(t) + \left(2i\omega + \frac{\omega_1}{Q_1}\right)\dot{p}_{10} + \ddot{p}_{10}\right\}e^{i\omega t}$$
$$= -\frac{\epsilon_0}{\epsilon}\frac{\partial^2}{\partial t^2}\int_{V_{\text{crystal}}} \frac{\gamma p_{10}(t)|E_{i0}^* \cdot \mathbf{E}_1|^2}{|\mathbf{E}_{i0}|^2 + \dfrac{1}{\epsilon}|p_{10}(t)\mathbf{E}_1(\mathbf{r})|^2} e^{i\omega t}\, dV \qquad (18.3\text{-}14)$$

At steady state $\dot{p}_{10}$ and $\ddot{p}_{10}$ vanish, $\partial/\partial t \to i\omega$, and $p_{10}(t) = p_{10} = \text{constant}$. The oscillation condition (18.3-14) becomes

$$(\omega_1^2 - \omega^2) + i\frac{\omega_1\omega}{Q_1} = \frac{\epsilon_0}{\epsilon}\omega^2\gamma f$$
$$= i\frac{\epsilon_0}{\epsilon}\omega^2 f \frac{\gamma_0}{1 + i(\omega - \omega_0)\tau} \qquad (18.3\text{-}15)$$

where in the second equality we used the zero-external-field ($E_0 = 0$) form for γ given by (18.3-12) and f is given by

$$f = \int_{V_{\text{crystal}}} \frac{|\mathbf{E}_{i0}^*(\mathbf{r}) \cdot \mathbf{E}_1(\mathbf{r})|^2}{|\mathbf{E}_{i0}(\mathbf{r})|^2 + \dfrac{1}{\epsilon}|p_{10}(\infty)\mathbf{E}_1(\mathbf{r})|^2} dV \qquad (18.3\text{-}16)$$

so that it is dimensionless and real.

The left-hand side of Equation (18.3-15) is a complex number that depends only on passive resonator parameters and the (yet unknown) oscillation frequency ω. The phase of the right-hand side of Equation (18.3-15) depends on $(\omega - \omega_0)$. The frequency ω will thus adjust itself relative to ω_0 to satisfy (18.3-15). Separating the real and imaginary parts of Equation (18.3-15) yields

$$\omega_1^2 - \omega^2 = \frac{\epsilon_0 f \gamma_0 \omega^2(\omega - \omega_0)\tau}{\epsilon[1 + (\omega - \omega_0)^2\tau^2]} \qquad (18.3\text{-}17a)$$

and

$$\frac{\omega_1\omega}{Q_1} = \frac{\epsilon_0 f \gamma_0 \omega^2}{\epsilon[1 + (\omega - \omega_0)^2\tau^2]} \qquad (18.3\text{-}17b)$$

Since $\omega \approx \omega_1 \approx \omega_0$, Equation (18.3-17a) can be approximated to a high degree of accuracy by

$$\omega_1 - \omega = \frac{\epsilon_0 f \gamma_0 \omega_0(\omega - \omega_0)\tau}{2\epsilon[1 + (\omega - \omega_0)^2\tau^2]} \qquad (18.3\text{-}18)$$

In the limit $t_1 \ll \tau$, where $t_1 = Q_1/\omega_1$ is the decay time constant of the photon density in the mode (with no photorefractive interaction), we can solve Equation (18.3-18) for ω and, using Equation (18.3-17b), obtain

$$(\omega - \omega_0) \cong 2\frac{t_1}{\tau}(\omega_1 - \omega_0) \tag{18.3-19}$$

This is our main result. It predicts a shift between the frequency of oscillation (ω) and that of the pumping field (ω_0). The frequency shift predicted by (18.3-19) was verified in a ring resonator pumped photorefractively as shown in Figure 18-12(a). A shift of the position of one of the mirrors changes the resonant frequency ω_1 of the ring resonator and causes a (near) linear shift of the oscillation frequency ω. The linewidth of γ is of the order of $1/\tau \sim 1$ Hz in $BaTiO_3$ so that the frequency pulling $(\omega - \omega_0)$ observed is of the order of a few Hz. A plot of the frequency shift $\omega - \omega_0$ vs. the mirror displacement for two different spatial modes is shown in Figure 18.12(b). The dependence of this shift on the parameters indicated in the equation was verified exper-

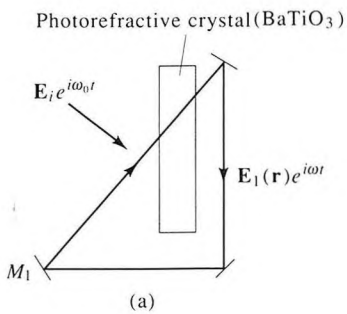

(a)

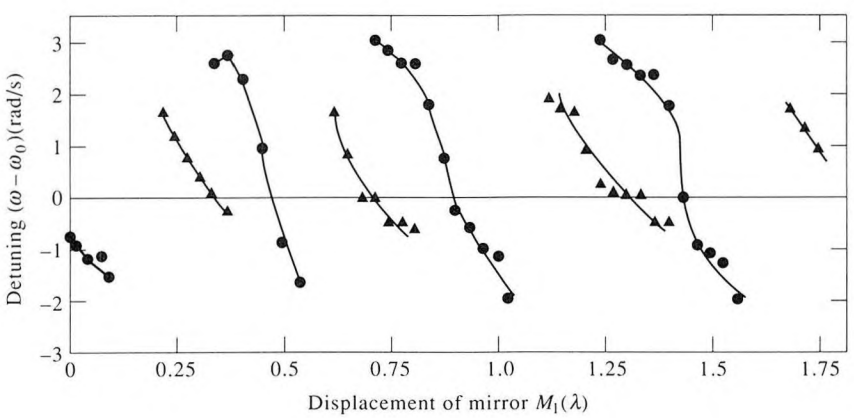

(b)

Figure 18-12 (a) Unidirectional ring resonator with two-beam gain provided by a photorefractive $BaTiO_3$ crystal pumped by an incoming beam E_i. (b) The observed frequency shift $(\omega - \omega_0)$ as a function of mirror displacement measured in wavelengths.

imentally and is shown in Figure 18-12 in a ring resonator pumped photorefractively.

Let us return next to the threshold condition (18.3-19). The parameter f is given by Equation (18.3-16) and can be written as

$$f \equiv \int \frac{|\mathbf{E}_{i0}^{*}(\mathbf{r}) \cdot \mathbf{E}_1(\mathbf{r})|^2}{|\mathbf{E}_{i0}(\mathbf{r})|^2 + |\mathbf{E}_{\text{osc}}(\mathbf{r})|^2}\, dV \tag{18.3-20}$$

$$\cong \frac{1}{1 + \dfrac{\langle |\mathbf{E}_{\text{osc}}|^2 \rangle}{\langle |\mathbf{E}_{i0}|^2 \rangle}} \int_{V_c} \frac{|\mathbf{E}_{i0}^{*}(\mathbf{r}) \cdot \mathbf{E}_1(\mathbf{r})|^2}{|\mathbf{E}_{i0}|^2}\, dV \tag{18.3-21}$$

where we used the first equation of (18.3-2) to write the oscillating electric field of the resonator mode as

$$\mathbf{E}_{\text{osc}}(\mathbf{r}) = -\frac{1}{\sqrt{\epsilon}}\, p_{10}(\infty)\mathbf{E}_1(\mathbf{r})$$

and $\langle\rangle$ to denote spatial averaging over the crystal volume. We can now rewrite f as

$$f = \frac{f_0}{1 + \dfrac{\langle |\mathbf{E}_{\text{osc}}|^2 \rangle}{\langle |\mathbf{E}_{i0}|^2 \rangle}} \tag{18.3-22}$$

where

$$f_0 \equiv \int \frac{|\mathbf{E}_{i0}^{*}(\mathbf{r}) \cdot \mathbf{E}_1(\mathbf{r})|^2}{|\mathbf{E}_{i0}|^2}\, dV \tag{18.3-23}$$

and (18.3-18) becomes

$$\frac{1}{\omega_1 t_1} = \frac{n^2 \gamma_0 f_0}{1 + 4(\omega_0 - \omega_1)^2 t_1^2} \left(\frac{1}{1 + \dfrac{\langle |\mathbf{E}_{\text{osc}}|^2 \rangle}{\langle |\mathbf{E}_{i0}|^2 \rangle}} \right) \tag{18.3-24}$$

where $t_1 = Q_1/\omega_1$ is the resonator-mode decay time constant. At the transient start of oscillation, the right-hand side of (18.3-24) with $|\mathbf{E}_{\text{osc}}| = 0$ must be larger than (or equal to) the left-hand side. Once oscillation starts, the term $|\mathbf{E}_{\text{osc}}|^2$ will grow until both sides are equal. The start-oscillation (threshold) condition is thus

$$\gamma_0 \geq \frac{1 + 4(\omega_0 - \omega_1)^2 t_1^2}{n^2 f_0 \omega_1 t_1} \tag{18.3-25}$$

and does not depend on the pumping intensity $|\mathbf{E}_{io}|^2$. The threshold value of γ_0 is smallest when $\omega = \omega_0$ and when the input mode is matched to the resonator mode, $\mathbf{E}_{i0}(\mathbf{r}) \propto \mathbf{E}_{\text{osc}}(\mathbf{r})$, a condition leading to a maximum value for f_0.

Equation (18.3-24) can be solved for the oscillating-field intensity inside the resonator

$$\langle|\mathbf{E}_{\text{osc}}|^2\rangle = \langle|\mathbf{E}_{i0}|^2\rangle \left[\frac{n^2\gamma_0 f_0 \omega_1 t_1}{1 + 4(\omega_0 - \omega_1)^2 t_1^2} - 1\right] \tag{18.3-26}$$

Before moving on we might recall the main result of this section. We have shown that two-beam coupling can be used to obtain oscillation when the amplified beam is a mode of a resonator. The oscillation frequency adjusts so as to satisfy the resonance phase conditions and consequently is not, in general, the same as that of the input pump wave. Another basic and important property is that the spatial profile of the input beam only plays a role, through the overlap integral (18.3-23), in the magnitude of the gain "seen" by the oscillating mode but does not, to the first order, affect its shape, which is determined by the resonator. We thus have a means of transferring power from a spatially "dirty" beam to a well-defined, "clean" resonator mode. In practice we can use this effect to increase the apparent brightness of a beam (watt-cm^{-2}-sr^{-1}) by orders of magnitudes [21].

18.4 APPLICATIONS OF PHOTOREFRACTIVE OSCILLATORS

In this section we will describe some generic applications of photorefractive oscillators. In principle almost any application that uses "conventional" phase conjugate reflectors, i.e., ones that depend on externally supplied pump waves (A_1 and A_2 in Figure 17-10) can also use a self-pumped phase conjugate mirror [16]. As a matter of fact, the dynamic distortion correction of a laser mode demonstrated in Figure 17-11 employs a self-pumped phase conjugate mirror consisting of the crystal c and the *single* mirror M_2.

Rotation Sensing

As a representative example of the applications of phase conjugate mirrors we take up the case of fiber rotation sensors [17, 18]. A rotation sensor based on the Sagnac effect is shown in Figure 18-13. The basic principle of such a sensor is that light propagating in a coiled fiber (coil radius = R) will undergo an extra phase shift

$$\phi = \frac{2\pi RL}{\lambda c}\,\Omega \tag{18.4-1}$$

where L is the length of the fiber, c, λ are the vacuum value of the velocity of light and the wavelength, respectively, and Ω the angular rotation rate (rad/s) about an axis normal to the plane of the loop. $\Omega > 0$ when the light propagates in the same sense as the rotation and is negative otherwise. Note that ϕ is independent of the refractive index n of the fiber material [17].

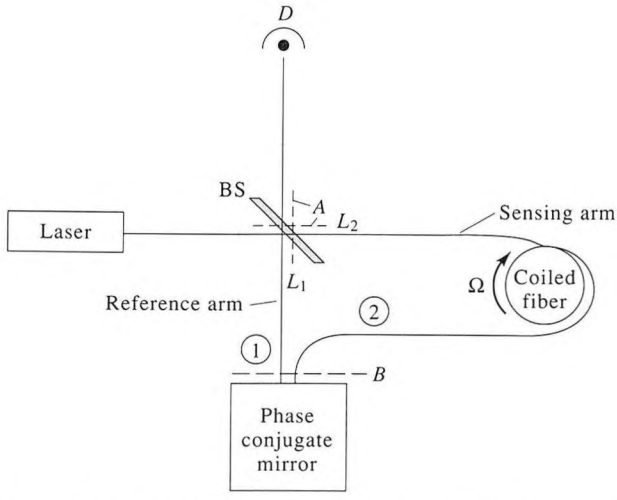

Figure 8-13 The generic configuration of an interferometric fiber rotation sensor employing the Sagnac effect and a self-pumped phase conjugate mirror.

The derivation of ϕ is based on relativistic considerations. The correct result, however, can be obtained almost rigorously, from a consideration of the effective elongation (shortening) of a fiber experienced by light propagating in the same (opposite) sense as the rotation.

In the interferometric arrangement of Figure 18-14 a beam splitter sends one part of the input beam through a coiled fiber (sensing arm) while the other portion of the split beam enters the "reference" uncoiled arm. Both beams are then reflected from a self-pumped phase conjugate mirror, retraverse their original path and recombine interferometrically at detector D. Consider first the beam in the sensing arm. On its forward path between planes A and B it undergoes a phase shift

$$\phi_1 = kL_2 + \frac{2\pi RL_2}{c\lambda}\,\Omega + \phi_{R2}(t) \qquad (18.4\text{-}2)$$

where $k = 2\pi n/\lambda$, and $\phi_{R2}(t)$ accounts for random ("noise") phase fluctuations in the sensing leg that are "slow" on the time scale of a round trip (these could be due, for example, to strain or temperature variations). The phase of the beam after reflection from the conjugator at point B is the reverse of the input phase plus an additional phase ϕ_c

$$\phi_2 = -kL_2 - \frac{2\pi RL_2}{c\lambda}\,\Omega - \phi_{R2}(t) + \phi_c[\Omega, kL_1, kL_2, \phi_{R1}(t), \phi_{R2}(t)] \qquad (18.4\text{-}3)$$

The last term ϕ_c in (18.4-3) is of fundamental importance. In the case of a single input (i.e., with the reference arm blocked-off) $\phi_c = 2kL_2$ and the overall phase delay $\phi_1 + \phi_2$ due to L_2 is $2kL_2$, as required by causality. In

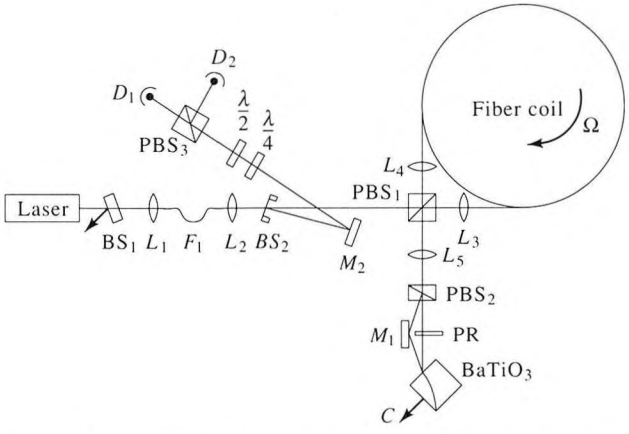

Figure 18-14 Experimental fiber-optic gyroscope setup using a self-pumped phase conjugate mirror. Instead of the two fibers in Figure 18-13, the experimental setup of this figure uses the two polarization modes of a polarization preserving fiber. (After Reference [18].)

the case of more than one input beam, the phase delay term ϕ_c is the same for all of them[3] [19], so that the relative phases of the beams are reversed, as required for phase conjugation, while the absolute phases are not. After retracing the original path, the sensing beam returns to A with a phase

$$\begin{aligned}\phi_{\text{sense}} &= \left[-kL_2 - \frac{2\pi RL_2}{c\lambda}\,\Omega - \phi_{R2}(t) + \phi_c[\Omega, kL_1, kL_2, \phi_{R1}(t), \phi_{R2}(t)]\right] \\ &\quad + \left(kL_2 - \frac{2\pi RL_2}{c\lambda}\,\Omega + \phi_{R2}(t)\right) \\ &= -\frac{4\pi RL_2}{c\lambda}\,\Omega + \phi_c[\Omega, kL_1, kL_2, \phi_{R1}(t), \phi_{R2}(t)] \qquad \text{(18.4-4)}\end{aligned}$$

note that the phase shift due to Ω has the opposite sign on the return trip since the sense of rotation relative to the beam is now reversed.

Repeating the same procedure in the case of the reference beam leads to a phase of the reflected beam at plane A

$$\begin{aligned}\phi_{\text{ref}} &= -[kL_1 + \phi_{R1}(t)] + \phi_c(\Omega, kL_1, kL_2, \phi_{R1}(t), \phi_{R2}(t) \\ &\quad + [kL_1 + \phi_{R1}(t)] \\ &= \phi_c(\Omega, kL_1, kL_2, \phi_{R1}(t), \phi_{R2}(t)) \qquad \text{(18.4-5)}\end{aligned}$$

[3]The crystal "regards" the multiplicity of input beams, which are coherent relative to each other, as a single, albeit complex, beam. The phase ϕ_c is thus due to the complex but *single* grating "written" in the crystal by this composite beam.

The interference output signal at D thus involves the phase difference

$$\phi_{\text{ref}} - \phi_{\text{sense}} = \frac{4\pi R L_2}{c\lambda}\,\Omega \tag{18.4-6}$$

from which the extraneous effects of phase fluctuations ϕ_{R1}, ϕ_{R2}, that usually limit the sensitivity of such sensors, disappeared.

A basic point that should have emerged from the preceding discussion is that although a passive (self-pumped) phase conjugate mirror does not reverse the absolute[4] phase of an incoming beam, it does reverse the *relative* phases of the Fourier components (partial plane waves) that make up the beam. This property is sufficient to guarantee wavefront reversal and enable various sensor applications [19]. Further discussion of this point is included in Problem 5 at the end of this chapter.

Mathematical and Logic Operations on Images

We have already discussed in Chapter 17 how nonlinear optical techniques can be used to perform spatial correlation, convolution, and other operations. In the following we will discuss some new mathematical operations that can be performed with passive (or externally pumped) phase conjugate mirrors.

Consider the configuration shown in Figure 18-15. A plane wave with

[4] "Absolute phase" here is taken to mean the phase relative to some coherent reference wave.

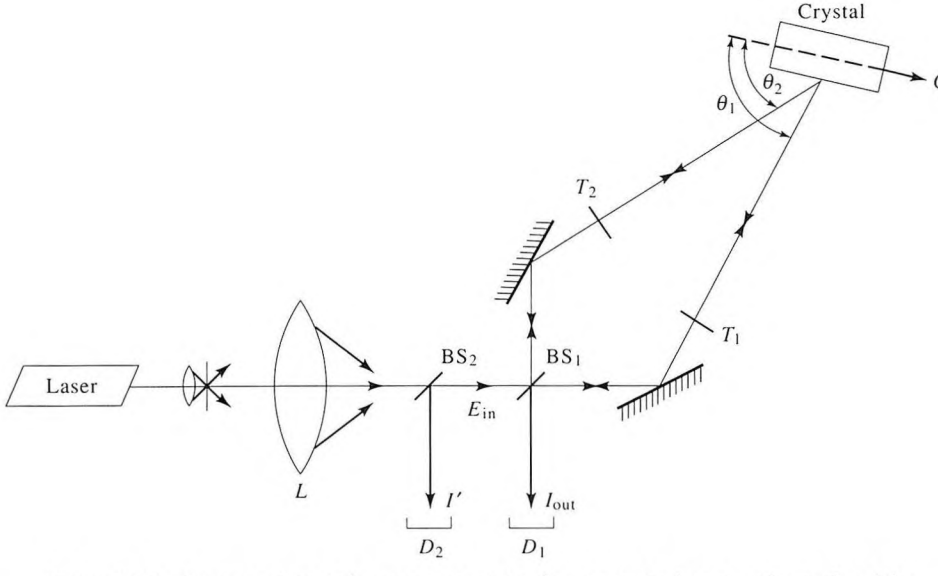

Figure 18-15 An experimental arrangement to demonstrate image subtraction (the "exclusive or" operation). (After Reference [20].)

amplitude E_{in} is split by a lossless beam splitter BS_1 whose reflection and transmission coefficients are equal to r and t, respectively. Let r′ and t′ be the amplitude reflection and transmission coefficients for waves incident from the opposite side of the beam splitter. Each of the two resulting (split) waves passes through a transparency with amplitude transmittance T_1 for beam 1 and T_2 for beam 2. The two beams are then reflected by a self-pumped phase conjugate mirror (PPCM) with phase conjugate amplitude reflectivity R. The phase conjugate beams recombine interferometrically at beam splitter BS_1 to form an output field. The total field at D_1 is

$$E_{out} \propto E_{in}^{*}\,[(rT_2)^{*}R\;T_2t + (tT_1)^{*}RT_1r'] = E_{in}^{*}R(r^{*}t)(|T_2|^2 - |T_1|^2) \qquad (18.4\text{-}7)$$

where we took advantage of the time reversibility condition (see Problem 9),

$$r't^{*} + r^{*}t = 0 \qquad (18.4\text{-}8)$$

The intensity at D_1 becomes

$$\begin{aligned} I_{out} \equiv |E_{out}|^2 &= |R|^2|T_1|^2 - |T_2|^2|^2|r^{*}t|^2 I_{in} \\ &\propto |T_1|^2 \mathbf{O} |T_2|^2 \end{aligned} \qquad (18.4\text{-}9)$$

where **O** represents the Boolean "exclusive or" operation. The field at D_1 is thus the difference (squared) of the intensity pattern of the two transparencies. Similarly the field intensity I' at D_2 is

$$\begin{aligned} I' &\propto |T_1|^2 + |r|^2(|T_2|^2 - |T_1|^2)|^2|R|^2 I_{in} \\ &\propto |T_1|^2 + |T_2|^2 \qquad \text{when } |r|^2 = .5 \end{aligned} \qquad (18.4\text{-}10)$$

Note that when $T_1 = e^{i\theta_1(\mathbf{x}_t)}$ and $T_2 = e^{i\theta_2(\mathbf{x}_t)}$, i.e., pure phase modulation, $I_{out} = 0$. This is at first sight, an amazing result. A little thought, however, will convince us that this is as it should be. When the transparencies are lossless (which is the case for $T_{1,2} = \exp[i\theta_{1,2}(\mathbf{x}_t)]$) a "time reversal" by the conjugator should result in a return field at the beam splitter BS_1 that is a time-reversed (phase conjugate) replica of the incoming field. Since no field entered BS_1 from the direction of D_1, none can emerge that propagate toward BS_1. Since in this case $|T_1| = |T_2| =$ constant, the vanishing of the field propagating toward D_1 comes about by destructive interference, point by point, of the two fields as expressed by (18.4-7). When T_1 and T_2 are, each, spatially intensity modulated the point by point destructive interference is no longer operative. A dark area in T_1 cannot, obviously, interfere with a bright spot on T_2. More globally, the path becomes lossy (or amplifying) and, except for the trivial case of uniform and equal, $|T_1| = |T_2|$, the time reversibility property of phase conjugation (see Section 17-1) does not hold. The striking advantage of the phase-conjugating interferometer described above is that the system works without any need to balance L_1 and L_2 or to maintain their path difference constant to within a small fraction of λ as is usually required with conventional interferometers.

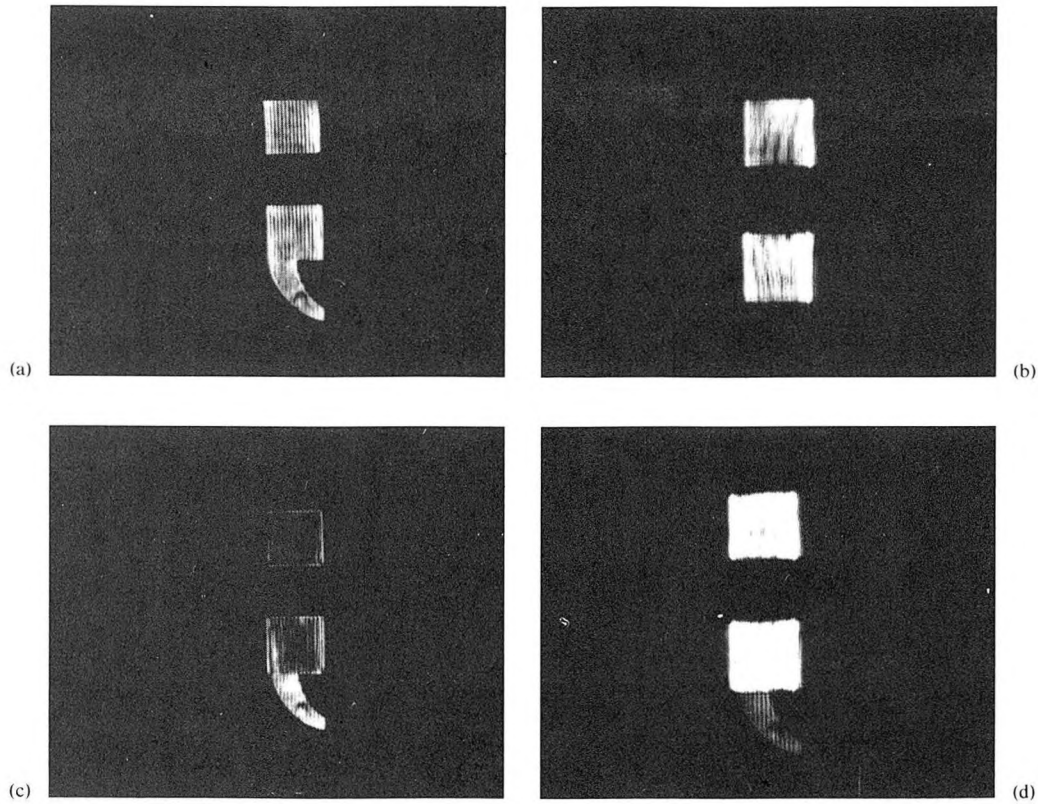

Figure 18-16 The results of image subtraction using the setup of Figure 18-15 (see text for details). (After Reference [20].)

Figure 18-16 shows the result of experiments using the setup of Figure 18-15. Figure 18-16(a) shows the image at D_2 of a semicolon transparency place at T_1 with beam 2 blocked and in (b) the image of a colon placed T_2 with path 1 blocked. Figure 18-16(c) shows the result of "subtraction" as observed at D_1, while (d) shows the image at D_2.

Problems

18.1 Obtain the expression for the diffraction efficiency of a fixed hologram as in (18.1-9) when a slight deviation from the Bragg condition exists, i.e.,

$$\Delta \equiv \mathbf{k}_2 - \mathbf{k}_1 - \mathbf{K} \neq 0$$

Consider the effects on the diffraction efficiency of:

a. A small angular departure (δ) of the incident beam from that of the Bragg condition.
b. A small deviation of the wavelength. [*Hint:* Using Figure 18-1(b) show that for $\delta \ll 1$ $(\mathbf{k}_2 - \mathbf{k}_1 - \mathbf{K}) \cdot \mathbf{r} \approx k\delta(\sin\theta)z$.]

18.2

a. Obtain an expression for the diffraction efficiency of a transmission hologram (Figure 18-1) as a function of $\Delta\ell$ where Δ is defined by

$$\Delta \equiv |\mathbf{k}_1 - \mathbf{k}_2 + \mathbf{K}|$$

and ℓ is the length of the hologram (in the z direction).
b. Plot the diffraction efficiency of a fixed hologram as a function of λ for a fixed incidence angle. Assume $\Delta = 0$ at some nominal λ_0.

18.3 Derive an expression for the diffraction efficiency $|A_1(0)/A_2(0)|^2$, of a reflection hologram as shown in the accompanying figure.

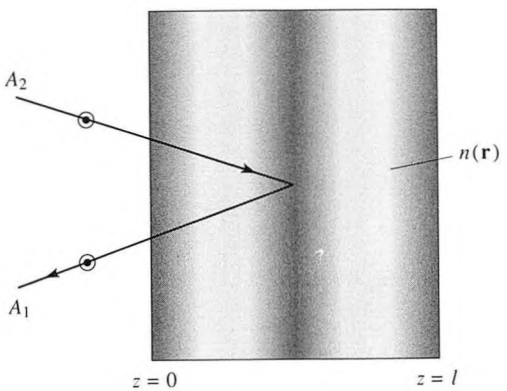

References

1. Kogelnik, H., "Coupled wave theory for thick hologram gratings," *Bell Syst. Tech. J.* 48:2909, 1969.
2. A. Yariv, *Quantum Electronics,* 3d ed. New York: Wiley, Chs. 16, 17.
3. Kukhtaerev, N. V., M. B. Markov, S. G. Odulov, M. S. Soskin, and V. L. Vinetsky, "Holographic storage in electrooptic crystals," Part I: Steady state, Part II: Beam coupling light amplification," *Ferroelectrics* 22:949, 1979.
4. Sayano, K., A. Yariv, and R. R. Neurgaonkar, "Reduction of the photorefractive response time in rhodium doped $Sr_{0.6}Ba_{0.4}Nb_2O_6$ with a dc field," *Opt. Lett.* 15:9–11, 1990.

5. Rakuljic, G., "Photorefractive properties and applications of BaTiO3 and tungsten bronze ferroelectrics," Ph.D. thesis, California Institute of Technology, Pasadena, California, 1987.
6. Huignard, J. P., J. P. Herriau, and G. Rivet, "Progress in photorefractive tungsten bronze crystals," *Opt. Lett.* 5:102, 1980.
7. Staebler, J. I., and D. L. Amodei, "Coupled-wave analysis of holographic storage in LiNbO3," *J. Appl. Phys.* 46:3510, 1975.
8. J. O. White, S. Kwong, M. C. Golomb, B. Fischer, and A. Yariv, "Wave propagation in photorefractive media," in *Topics in Applied Physics* 62: 101, Berlin: Springer-Verlag, 1989. This whole volume, edited by P. Guenther and J. P. Huignard consists of authoritative review papers, seven on various aspects of the photorefractive effect and its applications.
9. M. Cronin-Golomb, B. Fischer, J. O. White, and A. Yariv, "Passive (self-pumped) phase conjugate mirror," *Appl. Phys. Lett.* 41:689, 1982.
10. Feinberg, J., "Self pumped continuous wave phase conjugator using internal reflection," *Opt. Lett.* 7:486, 1982.
11. Kwong, S. K., M. Cronin-Golomb, and A. Yariv, "Oscillation with photorefractive gain," *IEEE J. Quant. Elec.* QE-22:1508, 1986.
12. Yariv, A., and S. K. Kwong, "Theory of Laser Oscillators with Photorefractive Gain," *IEEE J. Quant. Elec.* QE-22:1508, 1986. 13. Slater, J. C., *Microwave Electronics.* Princeton, N. J.: Van Nostrand, 1950.
14. Yariv, A., *Quantum Electronics,* 2d ed. (Wiley, New York 1975).
15. Special issue on Nonlinear Optical Phase Conjugation, *IEEE J. Quant. Elec.* 25, D. M. Pepper, ed., March 1989.
16. Kyuma, K., S. K. Kwong, M. Cronin-Golomb, and A. Yariv, "Principles and applications of optical phase conjugation in photorefractive materials," *Optoelectronics,* 2:1, 1987.
17. G. Joos, *Theoretical Physics* New York: Hefner, 1950, p. 471.
18. P. Yeh, I. McMichael, and M. Khroshevisan, "Phase conjugate fiber-optic gyro," *Appl. Opt.* 25:1029, 1986.
19. Y. Tomita, R. Yahalom, A. Yariv, "On the phase shift of a self-pumped phase conjugate mirror," *J. Opt. Soc. Am, B.*
20. Kwong, S. K., G. Rakuljic, and A. Yariv, "Real time image subtraction and 'exclusive or' operation using a self-pumped phase conjugate mirror," *Appl. Phys. Lett.* 48:201, 1986.
21. Kwong, S. K., and A. Yariv, "One-way real time wavefront converters," Appl. Phys. Lett. 48:9, 1986.